A Micro Aerial Vehicle with Precise Position and Attitude Sensors

Martin Rehak, Romain Mabillard & Jan Skaloud, Lausanne, Switzerland

Summary: This study shows the potential of navigation technologies in the field of position and orientation determination on a micro aerial vehicle (MAV), which weight does not exceed 5 kg. Although the MAV systems feature high flexibility and capability of flying into areas that are inhospitable or inaccessible to humans, the lack of precision in positioning and attitude estimation on-board decreases the gained value of the captured imagery. This limits their mode of operation to indirect georeferencing. This paper presents the development of a low cost MAV with navigation-sensor payload that shall assure a position and attitude control with accuracy from which either direct or integrated sensor orientation can benefit. After describing the hardware configuration and the synchronization of all measurements we present a case study that evaluates the performance of the positioning component and its application on integrated sensor orientation without ground control. There we show that thanks to the implementation of a multi-frequency, low power GNSS receiver, the system can potentially attain the mapping characteristics of much larger platforms flown on man-operated carriers while keeping the sensor size and weight suitable for MAV operations. The attitude accuracy of the developed board hosting several MEMS-IMUs is evaluated dynamically on a terrestrial vehicle using a reference (navigation grade) INS. Although this method offers continuous evaluation of the orientation accuracy and the obtained results are satisfactory with respect to the foreseen operations, this performance remains to be confirmed in a flight.

Zusammenfassung: *Ein MAV (Micro Aerial Vehicle) mit genauen Sensoren für die Positions- und Neigungsbestimmung.* Diese Untersuchung zeigt das Potenzial von Navigationssystemen für die Bestimmung der äußeren Orientierung von MAVs (Micro Aerial Vehicles) bis zu einem Gewicht von 5 kg. Die fehlende hochgenaue direkte Bestimmung der Orientierungsdaten der Bilder relativiert oft die Stärken von MAVs, z. B. ein Bildflug in Gebieten, die für den Menschen unzugänglich sind. Das bedeutet, dass immer eine indirekte Georeferenzierung, also die Bildtriangulation, erforderlich ist. In dem vorliegenden Artikel wird die Entwicklung einer low-cost Navigationseinheit für die direkte Georefenzierung von MAVs vorgestellt. Nach der Beschreibung der Hardware-Konfiguration und der Methode zur Synchronisationen aller Komponenten wird eine Fallstudie vorgestellt, die die Leistungsfähigkeit der Methode unter Beweis stellt und dabei die Ergebnisse der direkten Georefenzierung an bekannten Bodenpunkten prüft. Dabei zeigen die Autoren, dass der Multifrequenz GNSS-Empfänger mit geringer Leistungsaufnahme bezüglich der Genauigkeit mit Systemen, die auf bemannten Flugzeugen verwendet werden, vergleichbar ist. Die Genauigkeit der vom Autorenteam entwickelten Leiterplatte für die Neigungsmessung wurde durch eine 20-minütige Testfahrt mit einem Auto geprüft.

1 Introduction

1.1 *Problem Formulation*

Low-cost and low-weight unmanned aerial vehicle (UAV) systems with imaging capability have enjoyed a rapid development over the past years and are increasingly deployed as carriers for mapping purposes. They present a well-established tool for local-area remote sensing in the fields of agriculture, forestry, mining and hydrology as well as in the
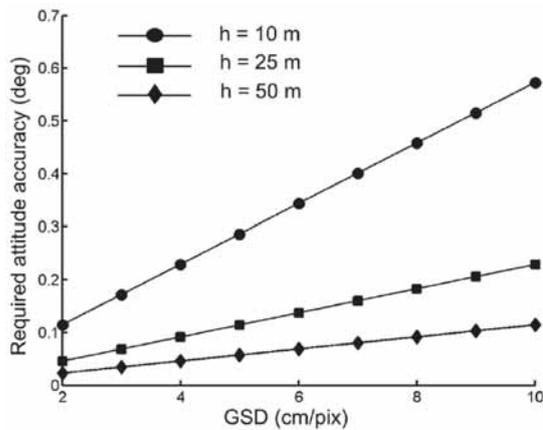
Fig. 1: Approximate requirements on attitude accuracy for direct sensor orientation on MAV at different flying heights above ground.
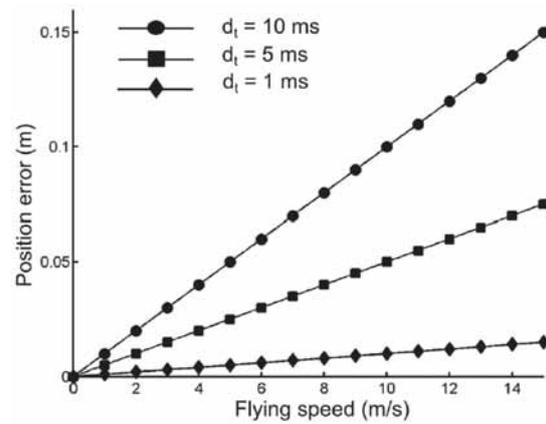
Fig. 2: Influence of synchronization errors d_t on aerial position determination as a function of MAV speed.

scientific research (REMONDINO et al. 2011). Although these systems allow a new way of data collection in the field of geomatics, they inherit an old, i.e. indirect, approach to sensor/image orientation. Indeed, most of the commercially available micro aerial vehicles (MAVs), e.g. AIBOTIX 2013, SENSEFLY 2013, TRIMBLE 2013, carry consumer-market non-metric cameras and single-frequency GPS receivers without precise carrier phase observations providing position accuracy at level of several metres in optimal conditions. That is indeed insufficient for large scale mapping projects and cadastral surveying for which accuracy at a 2–5 centi-metre-level is needed. Furthermore the quality of the employed inertial sensor, often part of a low-cost autopilot unit, is not sufficient for accurate attitude determination at a level of $\sigma_{att} = 0.01$ deg – 0.1 deg (Fig. 1).

Hence, missions with the need of accurate mapping require image acquisition in a block-structure with large forward and side overlaps, the existence of possibly many ground-control points (GCPs) as well as contrast in the sur-face texture. Although single-strip operations are theoretically possible, the requirement on the number and distribution of GCPs makes them impractical. Overall, the need of ground operations limits the mapping productivity of MAVs. Although the orientation requirements have a very wide range and the overall accu-racy on the ground is dependent on many as-pects, the acceptable attitude error is propor-

tional to the ground sampling distance (GSD) and inversely proportional to the flying height above ground as shown in Fig. 1. On the oth-er hand, the requirement on aerial position control is directly related to GSD. The state-of-the-art of kinematic carrier-phase differ-ential positioning is situated at 2 cm – 5 cm noise level. Apart from the navigation solution based on global navigation satellite systems (GNSS) and inertial measurement systems (INS), the results are also influenced by the imaging sensor quality and image resolution (NASSAR & EL-SHEIMY 2005).

The quality of the GNSS/INS solution is furthermore influenced by the precision of the synchronization with the imaging sensor. Fig. 2 shows the influence of given synchro-nization errors on position for different flying speeds.

The problem of determining exterior ori-entation parameters by direct observation of camera position and attitude has been exten-sively researched in the past (e.g. SKALOUD 1999, MOSTAFA et al. 2001, SKALOUD et al. 1996, COLOMINA 1999). However, only recent studies discuss this problem in the context of MAVs, e.g. EUGSTER & NEBIKER 2008, BLÀHA et al. 2011, BÄUMKER et al. 2011, PFEIFER et al. 2012, BÄUMKER et al. 2013, ELING et al. 2014.

In principle, the following conditions must be met for the correct integration of posi-tion and attitude sensors (SKALOUD 1999): 1) The position and orientation offsets between

a GNSS antenna, inertial measurement unit (IMU) and a sensor, i.e. a camera, a laser scanner etc., must be determined, 2) these offsets must remain constant during each mission and 3) the time stamping of all observations must be achieved with sufficient accuracy. To carry out these conditions, we have to pay special attention on the implementation of each system component and their mutual interconnection. Only a precise integration of all components ensures valuable results.

1.2 *Objectives*

In this paper we propose a GNSS/INS sensor payload for the sake of obtaining precise sensor orientation on a multi-rotor MAV. Although the current trend is to use the indirect approach, we can see a gradual rise up in the field of advanced sensor integration into larger UAV platforms, e.g. SWISS DRONE (2013). In a certain sense this evolution follows the classical airborne photogrammetric development (COLOMINA & MOLINA 2014) to which direct sensor orientation was conceptually introduced in the early nineties (SCHWARZ et al. 1993) together with the first experimental confirmation in photogrammetry (SKALOUD et al. 1994). The progress in the field of miniaturization of the inertial technology as well as GNSS receivers and antennae allows in principle to create a small-integrated system from of-the-shelf components. Nevertheless, the hardware implementation needs to be combined with state-of-the-art processing to fulfil the accuracy requirements for direct or integrated sensor orientation.

Our ultimate goal is to integrate advanced navigation devices, i.e. a multi-frequency/constellation GNSS receiver and redundant MEMS IMU to improve the mapping accuracy while minimizing the number of GCPs and enhancing the flying capability of a custom made MAV. In this paper we focus on the MAV development, physical integration, synchronization and quality evaluation of the navigation components. During practical tests we evaluate the accuracy of GNSS-base positions for direct determination of camera projection centres. We also asses the quality of attitude determination on board of a ground

vehicle using a reference IMU. The following part describes the development of the new MAV with an open-source autopilot. The third section concentrates on the sensor integration and implementation on the developed platform. Special attention is given to the parameter estimation of the redundant IMU, its calibration and integration on the MAV. The problem of camera synchronization is described and a method of the shutter-lag determination is presented. The fourth part is devoted to a case study where we describe the first results from platform operation. Finally, the last part draws conclusions and gives recommendations for future investigation.

2   **System Design**

The UAV platform market is getting more favourable every year in terms of price and performance. Manufactures produce sophisticated platforms, autopilots and camera gimbals. Nevertheless, the design is often closed and does not allow access or control of vital system components. Also the platform cannot be easily extended with additional sensors for the precise sensor orientation or for improving its capacity in autonomous navigation in case of interference or a denial of GNSS service. For these reasons we decided to build a new platform that shall be better suited for demanding mapping tasks.

2.1 *UAV Platform*

The custom design of a vertical take-off and landing (VTOL) MAV allows mounting the necessary devices needed to perform modern photogrammetry. The platform is equipped with eight brushless motors to enhance the payload capacity and to increase the redundancy in case of engine failure. The UAV accommodates appropriate sensors and an autopilot to perform stabilized and autonomous flights. The latter is based on a do-it-yourself project intensively developed during past years by the community of engineers and amateurs called Ardupilot APM 2.6 (3DROBOTICS 2013). This autopilot unit includes MEMS gyroscopes and accelerometers, a 3-axis mag-

netic sensor, a barometric pressure sensor and a single frequency low-cost GPS receiver. The cooperation of these navigation components allows horizontally and vertically stabilized positioning of the system as well as position hold, return to the launch site or other features including mission flights according to pre-planned trajectories.

The frame consists of carbon tubes and glass fibre base plates (Fig. 3). Special attention is given to the camera mount. This very light servo-powered gyro-stabilized camera holder keeps the equipment in level (or in selected inclination) during the flight. At the same time it dampens the vibrations from the engines. The camera can be tilted remotely to a desired angle along its horizontal axis. Fig. 4 shows the schematic location of the navigation components on the sensor mount.

The system is powered by high capacity lithium polymer (LiPo) batteries. Depending on the application and especially on the payload (1 kg – 1.5 kg), the flight times vary from 10 to 15 minutes. The system with all the equipment and additional sensors weighs 4.8 kg. The on-board control segment is an embedded micro-PC with an Atom processor connected to the Arduino autopilot. In its current configuration the PC governs the process of data acquisition and sets up the Ardupilot.

A significant challenge associated with MAV is their safety. To enhance the safety either for people and public infrastructure on the ground or also for the MAV itself, the multi-rotor is optionally equipped with a parachute to face emergency situations. The parachute is currently deployed manually by the operator. As a consequence of this additional payload of

**Fig. 3:** Octocopter with equipment (size: 80 cm in diameter).

240 grams, the flight times lower to approximately 8 minutes. Its functionality was tested during several field tests and the minimal flying altitude for a correct deployment was empirically estimated to be about 40 m.

The selected coaxial concept, two engines on each arm of the multi-rotor, has its specific advantages and disadvantages. Tab. 1 shows the basic characteristic of such a design (Mul-tirotor Forum 2013).

In manual mode the MAV helicopter can be operated by one pilot or as cooperation between two operators: one pilot and a second person responsible for the data acquisition. The system structure is universal as it can be (relatively easily) modified into a version with

Tab. 1: Advantages and disadvantages of a coaxial configuration.

+ Higher redundancy
+ Better orientation for a pilot
+ Compactness
+ More agile
+ Wider field of view for a camera
+ Better response to wind gusts
- Efficiency loss 15% – 30%
- Slightly worse stability
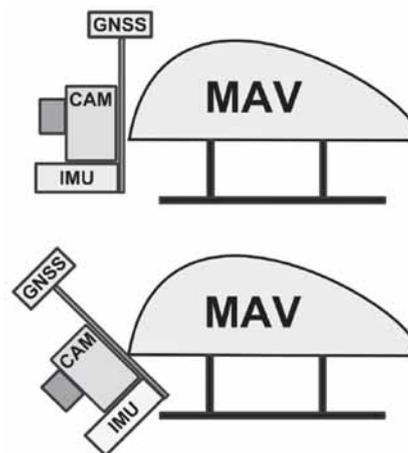
Fig. 4: Schematic sketch of the stabilized sensor mount for two distinct tilting angles.

only four motors or because the motors can be replaced by more powerful engines to increase the overall payload capacity.

2.2 *Optical Sensor*

The chosen optical sensor is the Sony NEX-5 camera. The quality of this mirror-less camera is comparable with a SLR camera despite being considerably smaller (only 111 × 59 × 38 mm³) and lighter (210 g without lens). These properties make it highly suitable for MAV platforms. The camera is equipped with a 16 mm fixed Sony lens, which has a reasonable optical quality given its size and weight and offers sufficient stability of the IO parameters through a mission. The camera is modified for better performance and integration into the MAV system. The on-board video-processing segment procures a digital to analogue conversion, video streaming and on-screen-display information of the current camera state as well as the telemetry data from the autopilot. The servo signal emitter triggers the camera shutter via an infra-red (IR) diode and a custom modification of hardware described in section 3.1 eliminates existing shutter lag and enables precise time synchronization with other navigation components. These modifications together with the external power supply convert this low-cost camera to a serious photogrammetric tool.

2.3 *Precise Positioning*

We employ a geodetic-grade multi-frequency and multi-constellation GPS/Glonass/Galileo OEM receiver (Javad 2013) with an appropriate antenna, RTK capability and 10 Hz sampling frequency. A similar setup is used as a base station for differential processing. The position of the MAV is determined in post-processing. However, in its current state it is ready for RTK solution and for further integration with the embedded PC and IMU.

2.4 *Inertial Measurement Unit*

Within a scope of this study we employ the in-house developed FPGA-board (Field-Programmable Gate Arrays) called Gecko4Nav comprising of four MEMS IMU chips, all precisely synchronized to the GPS time-reference (Kluter 2012). The Gecko4Nav contains two main components. The FPGA board handling the synchronization and data flow is connected to the state-of-the-art custom sensor board, equipped with various types of sensors. The main components are four NavChips IMUs that are software-combined to a redundant IMU (R-IMU). The performance characteristics for each sensor type provided by the manufacturers are shown in Tab. 2. The acquisition and control of the measurements are performed by the on-board firmware, which also governs the IMU sampling frequency. The latter can be selected by the user in the range from 250 to 500 Hz.

Dynamics encountered during the flight influence the behaviour of sensor errors. More specifically, its noise level may vary in time. Although such variations are not known a priori, the noise-level can be monitored on board thanks to multiple inertial sensors that are experiencing the same conditions. Indeed, the R-IMUs configuration improves the navigation performance on several levels (Waegli et al. 2010). First, it allows estimating the level of sensor noise directly from the data, which provides a correct view on the reality especially in a vibrating environment. Second, the noise

Tab. 2: Stochastic characteristics of the inertial sensors (InterSense 2013).

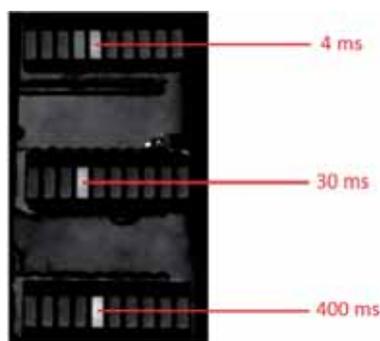| Sensor performance parameters	Gyroscopes	Accelerometers
In-run bias stability	10°/hr	0.05 mg
Scale factor	0.1 %	0.06%
Angle random walk	0.18°/√hr	0.03 m/s/√hr
Noise density	0.003°/s/√Hz	50 μg/√Hz

level of the overall system can be reduced by weighted combinations or mitigated directly in the navigation filter. Third, defective sensors can be detected and isolated via a Fault Detection and Isolation procedure (Guerrier et al. 2011). Finally, the overall performance of an R-IMU is superior to its individual inertial units.

3 Sensor Integration

3.1 *Time Synchronization of a low-cost Camera*

Precise time tagging of the camera shutter within the GPS time-scale is the prerequisite for annotating the acquired imagery with the position and attitude information derived from the on-board GNSS/R-IMU. With MAVs, the common way of image synchronization with the position is through the correlation between image acquisition time stored in an EXIF file and the GPS log. This method is sufficient for the indirect approach to the sensor orientation where the GPS antenna positions enter only during the image pre-selection and/or as an initial approximation for the bundle adjustment. As the precise knowledge of the EO parameters is mandatory for direct or integrated sensor orientation, a considerably more accurate method of synchronization had to be conceived.

The camera delay, or so-called shutter lag, is a feature which affects all consumer grade cameras and has a significant influence on the precision of synchronization. When the shutter button is pressed or a triggering signal is

sent, the camera may seem to take a photo instantly; however, there is a certain delay before a photo is actually taken. There are several ways to reduce this delay, but it is not possible to eliminate it completely. Even though the mission of the VTOL UAV can be programmed so that during the image acquisition the UAV hovers, the residual motion is not negligible. If the synchronization is not correct, this translates to an error in the parameters of the exterior orientation. Nevertheless, as long as the lag stays constant in time, it can be subtracted and thus corrected. A problem occurs with its instability or randomness.

In order to estimate the lag, we used a timer designed at the Czech Technical University (Jon et al. 2013). It sends a trigger signal to the camera at an optional interval, e.g. every two seconds, and at the same time it runs graphical time counters with a resolution of one millisecond (Fig. 5). The camera takes images with these counters and an automatic evaluation based on image processing determines their values at time of exposure. After initial testing summarized in Tab. 3 we concluded that the residual variations are too large and therefore made additional modifications. The relatively large delay has its origin in the shutter construction, whereas the IR-shutter is responsible for its variance.

Several options are viable in terms of change/modification of the triggering system or signalization of the shutter opening. The presented method is based on processing of the camera flash signal, which the camera sends at the exact moment when the shutter opens. This signal is further processed and time-tagged. Thanks to this modification, we managed to eliminate the inaccuracy of the built-in IR shutter and attained the desired accuracy of image time tagging.


Fig. 5: Determination of a camera lag using LED bar-graphs.

Tab. 3: Camera-lag statistics in a manual mode (STD = standard deviation).

Number of samples	88
Maximal delay	0.486 s
Minimal delay	0.406 s
Average delay	0.433 s
STD	0.013 s

The need of such modifications can be possibly eliminated by using industrial cameras, which are equipped with a sync port for the precise synchronization. On the other hand, these cameras are significantly more expensive and do not provide a comparable resolution for the same size, weight and price as the camera used here. In addition, an advantage of the Sony NEX-5 camera is the possibility of using various types of original or third party lenses with fixed focal length.

3.2 *IMU Synchronization*

The Gecko4Nav accommodates up to four NavChip IMUs on the same platform. The sampling of inertial observations at the same instance is a prerequisite for being able to exploit the benefits of redundancy and performance alleviation mentioned before. The Gecko4Nav features a synchronization module, which uses the pulse-per-second (PPS) signal issued by the GNSS receiver to adjust dynamically the drift within its crystal clock oscillator. This method ensures the continuity of the measurement procedure even if the PPS signal is lost. The synchronization was tested by placing the Gecko4Nav with the R-IMUs on top of a tactical grade inertial unit whose synchronization is known to be correct (SKA-LOUD et al. 2010). The latter served as a reference, although only approximate alignment with respect to MEMS IMUs was determined. The whole system was shaken along each axis and the dynamic responses were compared in time. As shown in Fig. 6, the four MEMS
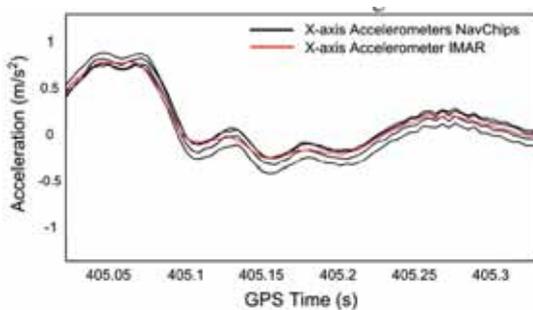
Fig. 6: Time-alignment of NavChip sensed specific force to the reference (iMAR-FSAS).

IMUs are synchronized well, both relative to each other and to the reference. Note that the depicted signal does not account for residual misalignments between the sensors.

3.3 *IMU Noise Parameters*

The acceleration and the angular speed measured by the MEMS IMUs are corrupted by relatively large errors of stochastic nature. These errors significantly influence the final navigation solution. Thus, they need to be filtered using a plausible model. The process of model building is not trivial at all. The following general error model can be formulated (TITTERTON & WESTON 2005):

$$\hat{l} = M_l \cdot \left(S_l \cdot l + b_l \right) + w_l \tag{1}$$

where $\hat{l}$ represents the adjusted measurements, l the observation and M_l the misalignment matrix. The diagonal matrix S_l contains the scale factors, b_l is the bias and w_l the measurement random errors.

3.4 *Random Errors without Bias*

The method of Allan variance (HOU & EL-SHEIMY 2004) is often used to determine the different types of random processes present in the inertial signal. In general, with the Allan variance only five processes are considered: quantization noise, white noise, bias instability, random walk, and the random rate ramp. The Allan variance is only used to build the model type, while the parameters of the model are estimated using the approach of generalized method of wavelet moments (GMWM) (GUERRIER et al. 2013). This estimation method is based on matching the empirical and model-based wavelet variances. The GMWM is able to handle complex error models for which other techniques such as the Allan variance or expectation-maximization (EM) algorithms fail or do not converge. The model consists of a mixture of several Gauss-Markov processes with white noise. The GMWM is used to estimate parameters of these processes, i.e. the variances and in case of Gauss-Markov processes also the correlation times.

3.5 *Deterministic Parts*

A multi-position calibration was used to estimate the deterministic errors such as the constant bias, the scale-factor and the non-orthogonality as shown in (1) (Syed et al. 2007). This method does not require any special mounting. It uses the combined effect of the local gravity and rotation vector to build the reference signals needed for calibration. The sensors do not have to be aligned to the local level frame. Nevertheless, it is necessary to have a redundant number of IMU rotations to estimate the errors by using a least-squares adjustment knowing that constrains can be imposed for accelerometers and gyroscopes:

$$f_1^2 + f_2^2 + f_3^2 - |g|^2 = 0 \qquad (2)$$

$$\omega_1^2 + \omega_2^2 + \omega_3^2 - |\omega|^2 = 0 \qquad (3)$$

Where $f_{1,2,3}$ are the specific forces measured along three axes (1,2,3), g is the true local gravity, $\omega_{1,2,3}$ are the angular rates measured along three axes, and ω is either the earth rotation rate or a known value from a rotation table. Once the model is built its parameters enter into the in-house developed navigation software that allows GNSS/R-IMU integration in different manners (Stebler & Skaloud 2013). By using redundancy in inertial sensors, the level of measurement noise can be estimated directly from the data itself and its level adapted dynamically by Kalman filtering/smoothing. This provides a better view of the reality while reducing the level of noise in the whole system. Furthermore, the expected overall navigation solution is improved thanks to the special mechanization/integration of inertial data. The choice of the GNSS/INS integration strategy is mainly guided by the a priori knowledge of the relative geometry between the individual IMUs, i.e. calibration vs. mission.

3.6 *Performance Evaluation of the R-IMU*

The performance of the R-IMU was evaluated during a kinematic ground test with respect to a reference IMU. The latter was a navigation grade INS (IXSEA 2013). Both units were rigidly mounted together with a GNSS antenna and attached to a car roof. The test drive lasted 20 minutes and was carried out in an area with good GNSS signal quality. The collected data were then processed by the custom software (Stebler & Skaloud 2013).

The bars in Fig. 7 represent the RMS values calculated from attitude differences between R-IMU and the reference. The dots and
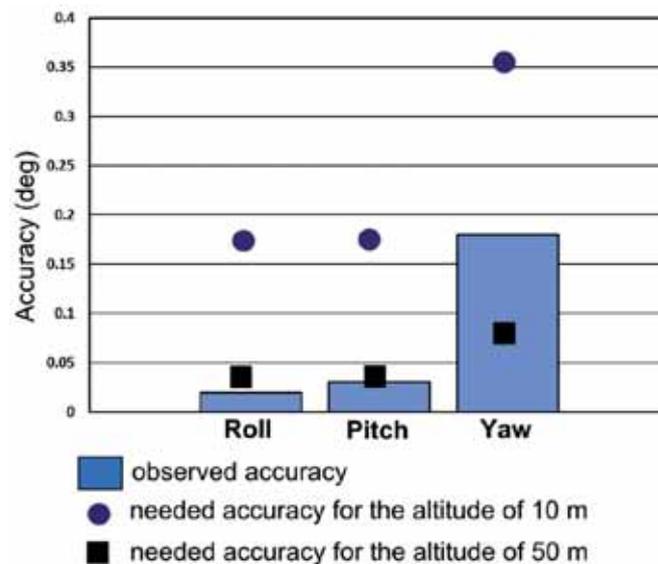
Fig. 7: R-IMU attitude accuracy obtained in a test on a moving car vs. required accuracy (1σ) to achieve σ$_{ground}$ = 3 cm for flying altitudes of 10 m and 50 m.

squares depict the required attitude accuracy for a direct sensor orientation with the current lens at two flying heights so that its influence on the ground is 3 cm (1σ). It can be seen that for the roll and pitch components the observed accuracy would be sufficient to contribute to direct/integrated sensor orientation. For the flying altitude of 50 m above ground the accuracy of the yaw angle obtained from the R-IMU would cause larger errors in case of direct orientation. However, its impact is mitigated in a strip/block structure due to observations of tie-points and perspective centre positions, respectively. It shall also be noted that for higher flying altitudes a lens with longer focal length would be used to preserve the ground-sampling distance.

4 Case Study

To evaluate the previously described development and to actually validate the existing integration of all system components, several field tests were carried out. Each test was performed for a specific task including tests on image quality, target recognition, camera calibration and synchronization of all components. However, this study is focused mainly on the quality of direct positioning. The quality of attitude control was evaluated only as presented in section 3 and is not the subject of this section.

4.1 Calibration Field

For the purpose of this study, we developed a calibration field (Fig. 8). Its size is approximately 30 m × 20 m with height differences of up to 2 m. 90 digitally coded targets were placed in a regular grid across the field. The positions of 25 targets were determined by tachymetric measurements and serve as ground control/check points. In such a setup we obtained high redundancy and an excellent distribution of measurements across the image plane. The estimation of the target centres in the image space was achieved by adopting the methodology commonly used by the research community of computer vision. Specifically, we have utilized the open-source software li-

Fig. 8: Calibration field.

brary ARToolkitPlus (Wagner & Schmalstieg 2007) to perform automatic target recognition. We employed the ARTag marker set due to its high marker library size, near-zero false positive identification rate as well as good accuracy potential for determining the target centres, which was reported to be 1/10 of a pixel (Fiala 2010). As the calibration field is situated in a relatively dense urban environment the quality of the satellite signal reception suffers from the limited visibility to the sky, which results in a relatively poorer geometry affecting mostly the vertical precision.

4.2 Data Acquisition

The performance of the proposed processing chain was evaluated during two separate flights. The first mission served specifically for the camera calibration, the second for the assessment of the synchronization and the overall quality of position control. The first flight resulted in a set of 92 images that were taken at two different height levels (5 m and 8 m) and with varying camera convergence angles. The second flight was performed several months later and had a flying pattern similar to traditional photogrammetric flights with a nadir-looking camera. This set consists of 68 images taken from the altitude of 10 m with a ground sampling distance of about 3 mm.

4.3 Camera Calibration

As the procedure of camera self-calibration is a well-established method, it is not repeated here; see, for example, Fraser (1997) for details. In this case all available ground control

points were processed together with the image measurements by a bundle-adjustment software (LICHTI & CHAPMAN 1997). The non-planar design of the target field, the variations of the camera convergence angles as well as the use of different flying heights above the target field decrease the correlation between the IO/EO parameters. Tab. 4 summarizes the precision of the most important results obtained from the camera self-calibration.

5 Results

The processing pipeline of the second flight was following that of classical airborne image processing with assisted carrier-phase differential GNSS. After the image acquisition and image processing, the image measurements were subsequently fed into a bundle adjustment (LICHTI & CHAPMAN 1997) together with the measured camera positions. The latter were obtained by interpolating between the 10 Hz GNSS solutions of carrier-phase differential results obtained by a professional software package. Self-developed Matlab scripts were used to carry out the assignment of images to the events exported from the receiver. The lever arm between the camera and GNSS antenna was measured with a calliper (Tab. 5). The R-IMU measurements were not considered in this process.

The processing was done with fixed interior orientation parameters that were estimated during the self-calibration project carried out much earlier. No ground control points were included in the adjustment. As mentioned previously, the prerequisite for such a comparison is the temporal-spatial stability between the camera and the navigation sensors. This was achieved by hard mounting the GNSS antenna and R-IMU to the camera gimbal. Even during the flight, the rigidity of the mount guarantees to maintain the stability of the relative positions (Fig. 4). The accuracy of the airborne positions was validated by comparing the GNSS-derived positions with those obtained by aerial triangulation (AT) in a separate adjustment project using 25 ground control points and re-estimated interior orientation parameters. Tab. 6 provides a summary of the quality of the GNSS data.

Tab. 4: Precision of the camera parameters after self-calibration.

Parameter	1σ
Principal point (x)	0.9 μm
Principal point (y)	2.0 μm
Principal distance	3.5 μm
K1 radial distortion	1.4 E-06
K2 radial distortion	7.9 E-09

Tab. 5: Measured lever arm.

Lever arm	Length (cm)
E_x	5.5
E_y	-1.1
E_z	12.9

Tab. 6: Summary of the quality of the GNSS data.

	Horizontal (m)	Vertical (m)
Mean estimated accuracy of GNSS positions	0.016	0.023
RMS of EO positions: estimated (AT + 25 GCPs) vs. GNSS measured	0.020	0.039
Maximal GNSS residual	0.069	0.099

Tab. 7: Residuals at 25 check points with GNSS-determined camera positions without using ground control points.

Residual	X (m)	Y (m)	Z (m)
MAX	0.028	0.043	0.079
MEAN	0.012	0.009	0.019
RMS	0.022	0.010	0.044

The characteristics of the residuals are presented in Fig. 9 where deviations in positions are depicted as points representing the differences between GNSS-derived positions of the camera perspective centres and those estimated by bundle adjustment with 25 ground control points.

As the lever-arm offset was subtracted from these differences, the depicted variations represent the Euclidean distance from the GNSS observations to the estimated camera perspective centres. We can see that their magnitude is not correlated with the flying speed. The observations lie within the interval given by the predicted incertitude of the estimated EO parameters (about 2 cm in horizontal, 3 cm – 4 cm in vertical direction). This confirms the sufficiently precise synchronization between the camera and GNSS receiver.

The statistics related to the residuals on all 25 check points are shown in Tab. 7. The overall RMS in position differences at the check points is 5 cm. The ground precision matches expectations and corresponds to the accuracy of kinematic carrier-phase differential GNSS. Despite that, an improvement can be still carried out as a part of the position error can be assigned to the GNSS signal quality, e.g. low SNR and higher than normal incertitude in height measurement.

The time-interval between the calibration and presented test flight was more than six months with several flights in between. This confirmed a sufficient stability of the IO parameters of the used camera-lens system.
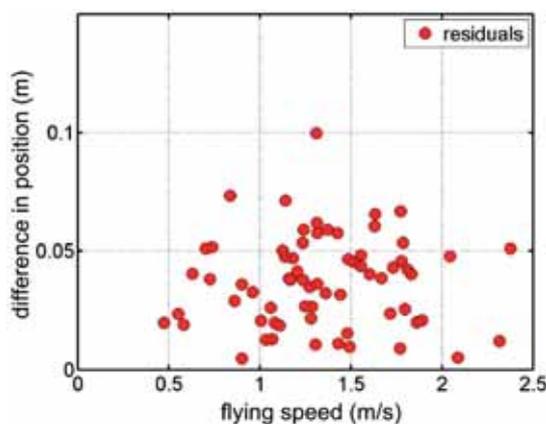
Fig. 9: Comparison of the GNSS-determined camera positions with the results of the AT.

6   Conclusion and Perspectives

This research aimed at proposing and investigating a novel approach in data acquisition with MAV. The outcomes from the bundle adjustment confirmed the correctness of the preceding development in terms of camera/GNSS integration. The most challenging part of the sensor integration and synchronization on the relative small and low cost UAV system was accomplished. The employed realization isolates the measuring devices from vibrations and provides stable spatial offsets between them. A small case study was performed to verify the quality of synchronization and the accuracy of camera position control. The latter is at 2 cm – 5 cm level which corresponds to the kinematic accuracy of a carrier-phase differential GNSS. The method of integrated sensor orientation allows performing mapping with cm-level accuracy without the need of ground control points. Future investigation will study the attainable attitude accuracy of the redundant MEMS IMU on-board the MAV. The performance of this sub-system is promising, as indicated by a car-based experiment reported in this paper.

References

Aibotix, 2013: http://www.aibotix.com/ (10.12.2013).

Bäumker, M. & Przybilla, H.-J., 2011: Investigation on the accuracy of the navigation data of unmanned aerial vehicles using example of the system Mikrokopter. – Conference on Unmanned Aerial Vehicles in Geomatics, Zurich, Switzerland.

Bäumker, M., Przybilla, H.-J. & Zurhorst, A., 2013: Enhancements in UAV flight control and sensor orientation. – Conference on Unmanned Aerial Vehicles in Geomatics, Rostock, Germany.

Blàha, M., Eisenbeiss, H., Grimm, D. & Limpach, P., 2011: Direct georeferencing with UAVs. – Conference on Unmanned Aerial Vehicles in Geomatics, Zurich, Switzerland.

Colomina, I., 1999: GPS, INS and Aerial Triangulation: what is the best way for the operational determination of photogrammetric image orientation? – ISPRS Conference Automatic Extraction of GIS Objects Digital Imagery, München.

COLOMINA, I. & MOLINA, P., 2014: Unmanned aerial systems for photogrammetry and remote sensing: A review. – ISPRS Journal of Photogrammetry and Remote Sensing **92** (6): 79–97.

ELING, C., KLINGBEIL, L., WIELAND, M. & KUHLMANN, H., 2014: Direct Georeferencing of Micro Aerial Vehicles – System Design, System Calibration and First Evaluation Tests. – PFG – Photogrammetrie, Fernerkundung, Geoinformation **2014** (4): 227–237.

EUGSTER, H. & NEBIKER, S., 2008: UAV-based augmented monitoring – real-time georeferencing and integration of video imagery with virtual globes. – ISPRS XXIth Congress **37** (B/1): 1229–1236, Beijing, China.

FIALA, M., 2010: Designing highly reliable fiducial markers. – IEEE Transactions on pattern analysis and machine intelligence **32** (7): 1317–1324.

FRASER, C.S., 1997: Digital camera self-calibration. – ISPRS Journal of Photogrammetry and Remote Sensing **4** (52):149–159.

GUERRIER, S., WAEGLI, A., SKALOUD, J. & VICTORIA-FESER, M.-P., 2011: Fault Detection and Isolation in Multiple MEMS-IMUs Configurations. – IEEE Transaction on aerospace and electronic systems **48:** 2015–2031.

GUERRIER, S., SKALOUD, J., STEBLER, Y. & VICTORIA-FESER, M.-P., 2013: Wavelet-variance-based estimation for composite stochastic processes. – Journal of the American Statistical Association **108:** 1021–1030.

HOU, H. & EL-SHEIMY, N., 2004: Modeling Inertial Sensors Errors Using Allan Variance. – Master thesis, University of Calgary, AL, Canada.

INTERSENSE, 2013: http://www.intersense.com/pages/16/16 (12.12.2013).

IXSEA, 2013: IXSEA AirINS. – http://www.ixsea.com/en/mobile_mapping_airborne_survey/3/airins.html (10.12.2013).

JAVAD, 2013: Javad TR-G3T datasheet. – www/javad.com/downloads/javadgnss/sheets/TR-G3T_Rev.5_Datasheet.pdf (5.12.2013).

JON, J., KOSTKA, B. & POSPISIL, J., 2013: Autonomous airship equipped with multi-sensor mapping platform. – 3D-ARCH 2013 – 3D Virtual Reconstruction and Visualization of Complex Architectures: 119–124, Trento, Italy.

KLUTER, T., 2012: Gecko4Nav. – Technical reference manual, revision 1.0.

LICHTI, D. & CHAPMAN, M.A., 1997: Constrained FEM self-calibration. – Photogrammetric Engineering & Remote Sensing **63** (9): 1111–1119.

MOSTAFA, M., HUTTON, J. & REID, B., 2001: GPS/IMU products – the Applanix approach. – Photogrammetric Week: 63–83, Wichmann, Heidelberg.

MULTIROTOR FORUM, 2013: http://www.multirotorforums.com/showthread.php?4015-X8-vs-flat-octo-redundancy-comparison (13.4.2014).

NASSAR, S. & EL-SHEIMY, N., 2005: Sensor Integration and Image Georeferencing for Airborne 3D Mapping Applications. – ISPRS International WG 1/2 Workshop 2005: 3D Mapping from InSAR and LiDAR, Banff, AL, Canada.

PFEIFER, N., GLIRA, P. & BRIESE, C. 2012: Direct georeferencing with on board navigation components of light weight UAV platforms. – ISPRS XXIIth Congress 39 (B/7), Melbourne, Australia.

REMONDINO, F., BARAZZETTI, L., NEX, F., SCAIONI, M. & SARAZZI, D., 2011: UAV photogrammetry for mapping and 3D modeling – current status and future perspectives. – Conference on Unmanned Aerial Vehicles in Geomatics, Zurich, Switzerland.

SCHWARZ, K.P., CHAPMAN, M., CANNON, M. & GONG, P., 1993: An integrated INS/GPS approach to the georeferencing of remotely sensed data. – Photogrammetric Engineering & Remote Sensing **59** (11): 1667–1674.

SENSEFLY, 2013: Ebee. – https://www.sensefly.com/drones/overview.html (10.12.2013).

SKALOUD, J., COSANDIER, D., SCHWARZ, K.P. & CHAPMAN, M., 1994: GPS/INS orientation accuracy derived from a medium scale photogrammetry test. – International symposium on kinematic systems in geodesy, Geodesy and navigation, KIS94, Banff, AL, Canada.

SKALOUD, J., CRAMER, M. & SCHWARZ, K.P., 1996: Exterior orientation by direct measurements of camera position and attitude. – International archives of photogrammetry and remote sensing **31** (B3): 125–130, Vienna, Austria.

SKALOUD, J., 1999: Problems in Direct-Georeferencing by INS/DGPS in the airborne environment. – ISPRS Workshop on Direct versus indirect methods of sensor orientation, WG III/1, http://infoscience.epfl.ch/record/29150 (1.5.2014).

SKALOUD, J., SCHAER, P., STEBLER, Y. & TOME, P., 2010: Real-time registration of airborne laser data with sub-decimeter accuracy. – ISPRS Journal of Photogrammetry and Remote Sensing **65** (2): 208–217.

STEBLER, Y. & SKALOUD, J., 2013: Modeling and processing approaches for integrated inertial navigation. – PhD thesis, EPFL, Lausanne, Switzerland.

SWISSDRONE, 2013: Dragon 35, http://www.swissdrones.com/SwissDrones_AG/Products.html (5.4.2013).

Syed, Z., Aggarwal, P., Goodall, C., Niu, X. & El-Sheimy, N., 2007: A new multi-position calibration method for MEMS inertial navigation systems. – Measurement science and technology **18:** 1897–1907.

Titterton, D. & Weston, J., 2005: Strapdown inertial navigation technology. – 2nd edition, ISBN 0863413587.

Trimble, 2013: UX5. – http://uas.trimble.com/ (5.12.2013).

Wagner, D. & Schmalstieg, D., 2007: ARToolkitPlus for pose tracking on mobile devices. – 12th Computer Vision Winter Workshop, Graz, Austria.

Waegli, A., Skaloud, J., Guerrier, S., Parés, M.E. & Colomina, I., 2010: Noise reduction and estimation in multiple micro-electro-mechanical inertial system. – Measurement science and technology **21**.

3DRobotics, 2013: Ardupilot Mega 2.5, http://www.store.3drobotics.com (10.4.2013).

Address of the Authors:

Ing. Martin Rehak, Ing. Romain Mabillard & Dr. Jan Skaloud, École Polytechnique Fédérale de Lausanne (EPFL), Geodetic Engineering Laboratory (TOPO), CH-1015 Lausanne, Tel.: +41-21-693-2756, -2755, -2753, Fax: +41-21-693-5740, e-mail: {martin.rehak}{romain.mabillard}{jan.skaloud}@epfl.ch